Journal of Nondestructive Evaluation (2024) 43:74
https://doi.org/10.1007/s10921-024-01096-3

Phased Array Ultrasonic Testing on Thick Glass Fiber Reinforced Thermoplastic Composite Pipe Implementing the Classical Time-Corrected Gain Method

Mohd Fadzil Mohd Tahir[1] · **Andreas T. Echtermeyer**[1]

Received: 26 January 2024 / Accepted: 20 May 2024 / Published online: 7 June 2024

Abstract
Thermoplastic composite pipe is gaining popularity in the oil and gas and renewable energy industries as an alternative to traditional metal pipe mainly due to its capability of being spooled onto a reel and exceptional corrosion resistance properties. Despite its corrosion-proof nature, this material remains susceptible to various defects, such as delamination, fiber breakage, matrix degradation and deformation. This study employed the phased array ultrasonic testing technique with the implementation of the classical time-corrected gain method to compensate for the significant spatial signal attenuation beyond the first interface layer in the thick multi-layered thermoplastic composite pipe. Initially, the ultrasonic signals from the interface layers and back wall were detected with good signal-to-noise ratios. Subsequently, flat-bottom holes of varying depths, simulating one-sided delamination, were bored and the proposed method effectively identified ultrasonic signals from these holes, clearly distinguishing them from the background noise and interface layer signals. Finally, a defect deliberately fabricated within the composite laminate layers during the pipe manufacturing process was successfully identified. Subsequently, this fabricated defect was visualized in a three-dimensional representation using the X-ray computed tomography for a qualitative and quantitative comparison with the proposed ultrasonic method, showing a high level of agreement.

Keywords Thermoplastic composite · Glass-fiber composite · Thick composite · Phased array ultrasonic · Time-corrected gain · Non-destructive testing

1 Introduction

In the early 21st Century, flexible thermoplastic composite pipe (TCP) set out to leave its footprint in marine applications of the oil and gas industry, such as flowlines and jumpers in subsea production systems. In the future hydrogen transport of the renewable energy sector, TCP provides a promising alternative to steel because it is corrosion-resistant, has superior fatigue life, costs lower in total installation, and reduces maintenance requirements, resulting in higher uptime [1]. Additionally, previous studies have reported that non-metallic pipes generate lower carbon and energy footprint than the metallic equivalent [2, 3]. As a result, the idea of such a replacement offers an eco-friendlier solution.

In parallel with the increasing trend of replacing metal pipes with TCP in the oil and gas and renewable energy sectors, there is still the need for developing a piping integrity management system that includes reliable inspection and monitoring methods for detecting discontinuities and damages in the piping structure during the manufacturing stage and in-service [4]. Melt-fuse engineering process on TCP creates an acoustically compatible bond between different types of layers that makes defect detection and characterization using the widely used ultrasonic testing (UT) method technically possible. However, there were only a few attempts to study the UT capability for this specific application on particularly thick composite structures composed of different types of layers, like fiber-reinforced plastic piping structures [4] or hybrid polymer matrix composites [5].

✉ Mohd Fadzil Mohd Tahir
mohd.f.b.m.tahir@ntnu.no

[1] Department of Mechanical and Industrial Engineering, NTNU, Richard Birkelands vei 2B, Trondheim 7491, Norway

Historically, UT machines were designed and developed to detect anomalies in homogeneous and isotropic materials, like metals. In general, the existing UT machines available on the market today are not ideally suited to inspect thick composite materials comprising two or more different layers. When inspecting highly attenuating composite materials, the UT technique suffers significantly from the high attenuation of sound waves due to absorption in the polymer matrix material, which could be up to four orders of magnitude greater than in metals [6] and scattering in random directions after reflection at interfaces between the fiber and matrix materials [7]. The increasing application of composite materials in the aerospace, aircraft, and automotive industries has created a demand for non-destructive testing (NDT) techniques to check the soundness of structural integrity.

Considering the limitations outlined above, most of the previous works studied the UT capability in detecting defects such as delamination [8–12] or barely visible impact damage [12–17] in thin monolithic composite structures, typically less than 10 mm. The orientation of artificial delamination was made almost perfectly perpendicular to the propagation of the longitudinal wave, making it possible to reflect most of the ultrasonic energy to the transducer in a pulse-echo configuration [9–15]. The main advantage of the pulse-echo configuration is that access to only one side of the inspected object is required compared to the through-transmission configuration, in which the receiver is located on the other side, and the technique works in detection mode only [8, 9, 16, 17].

Limited research has been conducted to explore the feasibility of utilizing the UT technique on thick wall composite structures, typically exceeding 20 mm, whose application is predominantly for oil and gas and renewable energy industries [18–21]. However, the thick composite samples used in the previous works were made of merely multiple composite laminate layers without considering the presence of the outer and inner polymer protective layers, which are crucial for protecting the load-bearing composite laminate layers from the harsh environment in the field. Phased array ultrasonic testing (PAUT) method was implemented in the investigation because PAUT transducers generally outperform single-element ultrasonic testing (SEUT) transducers in such a way that the signal attenuation improves as fewer gain values are required even though the signal-to-noise (SNR) is lower, which is attributed to the interference of the signals for each element [18, 22].

This paper aims to study the possibility of using the PAUT technique to inspect a thick multi-layered TCP made of thermoplastic high-density polyethylene (HDPE) material and glass fiber reinforcement by implementing the classical time-corrected gain (TCG) method to compensate for the significant signal dissipation beyond the first interface layer. The reliability of defect detection using the proposed method was investigated and verified. Defect visualization in a three-dimensional image was realized using an imaging-based NDT technique, namely X-ray computed tomography (CT) scan, for qualitative and quantitative comparison with the UT results obtained by the proposed method.

2 Preparation of Test Specimens

The TCP sample used in this work consists of three layers of different compositions: an outer cover, composite laminate layers, and an inner liner. They are melt-fused in a curated heating process to ensure strong and durable bonding, creating two interface layers between the cover and the composite laminate and between the liner and the composite laminate layers. The outer cover and inner liner are made of thermoplastic HDPE materials. The multiple composite laminate layers consist of glass fiber reinforcement and the same HDPE materials used in the cover and liner layers as the matrix. All these pipe components and their thicknesses are illustrated in Fig. 1 from the PAUT transducer's perspective.

The PAUT transducer scanned from the outer side of the TCP samples. The TCP samples were cut open in half along their axial center so that flat bottom holes (FBHs) of 7 mm in diameter, which is 1 mm smaller than half the size of the transducer's active aperture, were then drilled at various depths from the inner side of the sample, as illustrated in Fig. 2. FBHs with known depths help assess UT's capabilities in detecting defects in multi-layered TCP as they resemble one-sided delamination within the composite laminate layers and thinning in the thermoplastic outer cover or inner liner layer.

Additionally, a defect within the composite laminate layers was introduced during the pipe manufacturing. The presence of this fabricated defect was not revealed by the pipe manufacturer in advanced. It was assumed that the defect was created on the composite laminate layers before the HDPE outer cover layer was applied on it. Hence, the defect area of the composite laminate was filled with the thermoplastic material, making it invisible from the outside. Unlike the FBHs, the orientation of this defect was random, and the capability of the proposed method in detecting damage unfavorably oriented to ultrasonic wave propagation was also studied.

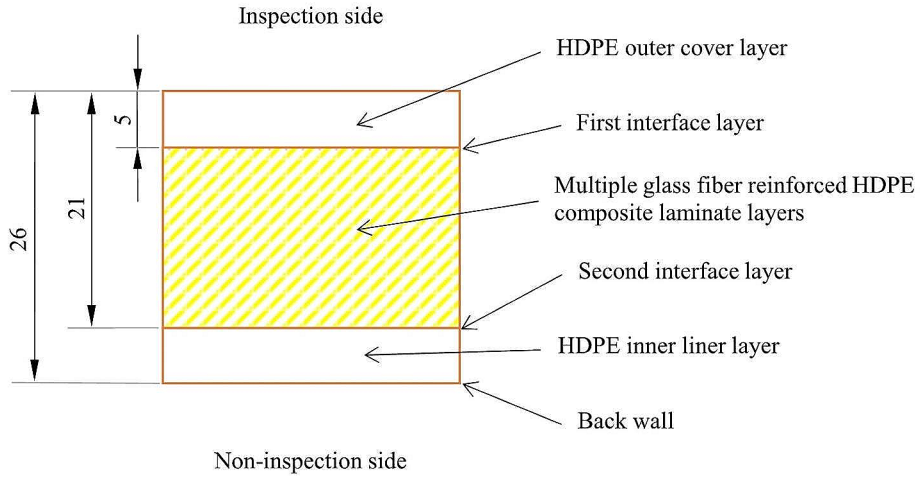

Fig. 1 Cross-sectional view of the TCP sample. Measurements are in mm

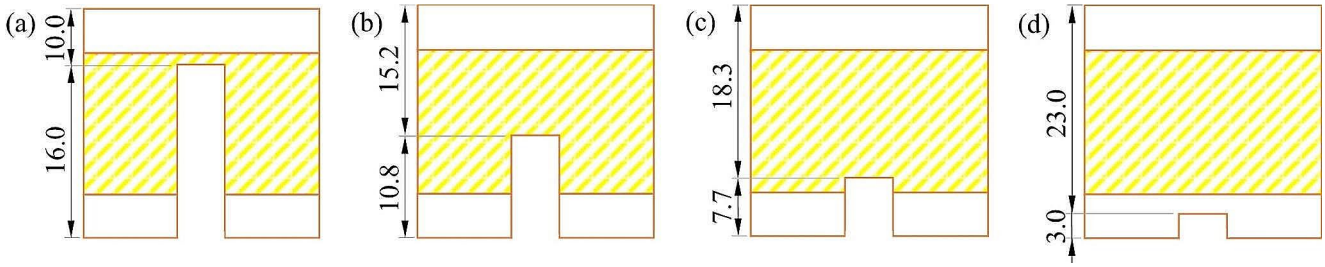

Fig. 2 Flat bottom holes, (**a**) FBH-1, (**b**) FBH-2, (**c**) FBH-3, and (**d**) FBH-4, were drilled from the inner side of the TCP samples. Measurements are in mm

3 Experimental Method

3.1 UT Method

A 16-element linear-array PAUT transducer from the Olympus A24 probe series having a 4 MHz center frequency, 16 mm active aperture, and 1 mm pitch was used. A 0.5 mm thick urethane disc was attached to the transducer face using a protective membrane retaining ring to protect it from abrasion or scratch during scanning. The raw data was acquired through the Olympus OmniScan SX flaw detector compatible with the PAUT application and transferred to the PC for post-inspection data analysis using the OmniPC 5 software, a so-called Freeware and comes as a complimentary companion software for the Olympus OmniScan series [23].

3.1.1 Focal Law Settings

In this work, the ultrasonic beam was unfocused, but the size of the virtual probe aperture (VPA) was varied to study the effect of using different beam size by grouping and pulsing different number of elements in the array on the detection capability of interface layers, back wall, and defects in the TCP samples. This variation was achieved by arithmetically increasing the element quantity from 4 to 8, 12, and 16. However, a maximum of 16-element VPA in a PAUT transducer with a 16-element active aperture would only provide a single waveform data as if an SEUT was utilized. Consequently, E-scan data could not be generated for real-time cross-sectional overview. Hence, the highest element quantity selected was reduced to 15 instead of 16. By stepping one element at a time over a 16-element span in the ultrasonic array set, the total number of VPAs generated for element quantity of 4, 8, 12, and 15 was 13, 9, 5, and 2, respectively.

3.1.2 Sound Velocity Calibration

The calibration of sound velocity was carried out on the TCP sample using the two-point calibration method, referring to the known depths of the first interface layer, the second interface layer, and the back wall. In the TCP, the sound wave travels within more than one dissimilar material with different material compositions having slightly different velocities due to differences in density and elasticity [5, 7]. However, the instrument's settings allow for only a single velocity value to be inputted. Consequently, the velocity

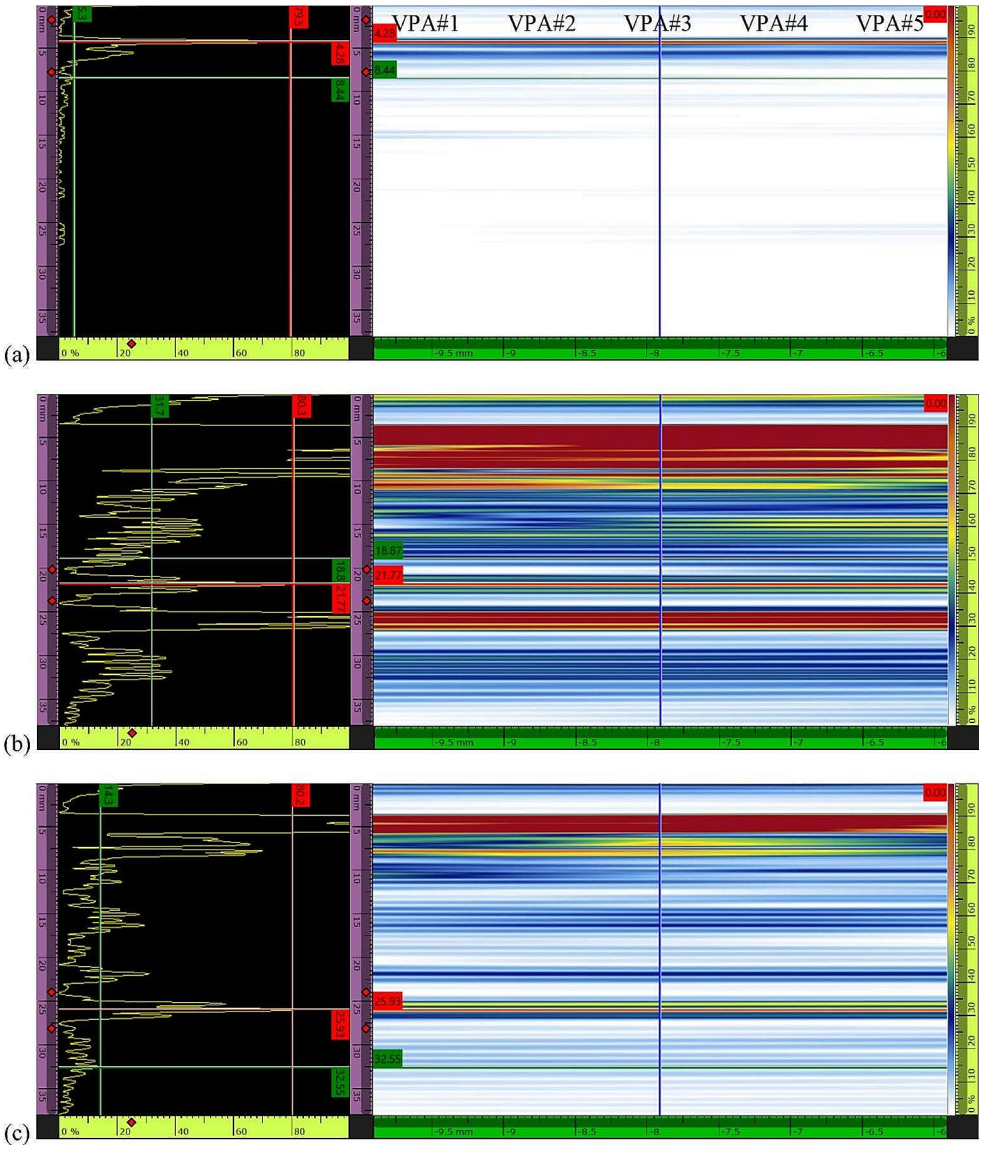

Fig. 3 Typical A-scan (left) and E-scan (right) views for the signal of the (**a**) first interface layer, (**b**) second interface layer, and (**c**) back wall at the defect-free area of the TCP sample marked by the red cursor (Element Quantity = 12)

measured using this approach was considered an average velocity value.

Initially, the instrument's gain setting was configured so that the signal from the first interface layer reached approximately 80% of the full-screen height (FSH), which was measured by an electronic gate positioned over the respective pulse width in the A-scan view. However, this gate was subsequently removed and substituted with the red cursor to minimize excessive indicators in an image, as shown in Fig. 3(a). This cursor indicated both the maximum amplitude height and the depth location of the first interface layer. The corresponding outer cover layer was considered the minimum thickness reference for the two-point calibration. After that, the gain setting was further increased to detect signals from the second interface layer and back wall to establish maximum thickness references. The red cursors in Fig. 3(b) and (c) marked both the maximum amplitude height, aligning closely with 80% of the FSH as measured by the virtual electronic gate positioned over the corresponding pulse width, and depth location of these two signals, respectively. The calibration was iteratively performed, considering two different maximum thickness references for each focal law, to compensate for element-to-element sensitivity variations in the ultrasonic array [7] before a single average velocity value was determined, as listed in Table 1.

Table 1 Measured average sound velocity in TCP sample for each focal law

Element quantity in each VPA	Velocity settings [m/s]
4	2405.3
8	2378.9
12	2378.9
15	2433.1

In polymer and polymer composite materials, variations in sound velocity may occur due to material heterogeneity, which leads to differences in density, stiffness, and acoustic impedance within the materials. Additionally, voids, porosity, or imperfections resulting from the manufacturing processes or material inconsistencies can further influence wave propagation. These irregularities can cause reflections and scattering, impacting the acoustic behavior of the material, and leading to variations in the measured sound velocity. In this study, the calibrated sound velocities obtained by different VPA sizes revealed a mean value of 2399.05 m/s, with a standard deviation of 25.89 m/s.

3.1.3 TCG Method

A classical method for system calibration and defect evaluation known as the TCG method (also known as time-varied gain), which reliably compensates for the severe spatial signal attenuation in multi-layered TCP, is proposed in this work. This method implements the partial increment of system gain with time so that the successive signal amplitudes requiring evaluation are at the same height as the first signal amplitude regardless of their distance. In general, the sound attenuation in polymer composite material is in the order of four magnitude higher than that in metal [6]. However, the beneficial consequence of this inherent limitation with regards to the implementation of the TCG method is that the repeated signal of the first interface layer, which would superimpose with the defect signal located beyond it, is meager and negligible, as shown in Fig. 3(a).

3.1.4 SNR Assessment and Signal Amplitude Gain Measurement before Implementing the TCG Settings

For a received signal to be called an indication, UT often follows the practical minimum requirement for SNR of 3:1 or 10 dB using the formula:

$$dB = 20 \times \log_{10}\frac{A_1}{A_2} \tag{1}$$

where A_1 and A_2 are the maximum signal and noise amplitude, respectively [24]. In this study, these values were determined by placing the electronic gate over the respective pulse width in the A-scan view. Then, this gate was removed and replaced by the red and green cursors, which marked the depth position and maximum height of the signal of interest and background noise, respectively, as shown in Fig. 3. During the initial gain setting, where the signal of the first interface layer reached approximately 80% of the FSH, it was evident that not only did the signals from the second interface layer and back wall disappear, but also did the repeated signal (second echo) of the first interface layer as well due to the severe attenuation of the sound beam, as shown in Fig. 3(a). The notable advantage of this occurrence was that when the gain setting is further increased to bring the signals of the second interface layer and back wall up to 80% of the FSH, the unwanted repeated signal would not appear, as shown in Fig. 3(b) and (c).

When assessing the SNR of the first interface layer signal, the maximum noise level was identified shortly after the pulse width, approximately 5 mm from the signal's peak amplitude, as indicated by the green cursor in Fig. 3(a). Subsequently, upon significantly increasing the instrument's gain until the signal of the second interface layer reached around 80% of the FSH, the background noise amplitude significantly increased as well. The noise originated from the combination of the multiple sound reflections within the composite laminate layers and the emerging reflected backward energy from the piezoelectric elements within the transducer [22, 25], which appeared at an earlier distance of approximately 16 mm for this setting. However, this study accounted for the former and disregarded the latter for the SNR assessment of the second interface layer signal prior to the TCG implementation. This consideration explained why the selected maximum noise was located a few millimeters after 16 mm and the values indicated by the green cursor in Fig. 3(b) were determined by the virtual electronic gate positioned after the disregarded noise signal. Additionally, the apparent signal right after the second interface layer belonged to the back wall and thus was not considered the respective noise. Consequently, the SNR for the second interface layer was measured to be less than 3 to 1.

Conversely, the SNR for the back wall was observed to be higher than that of the second interface layer because the increased background noise from the laminate layers was relatively more distant. It is worth noting that the instrument's gain was slightly reduced from the previous step of bringing the signal of the second interface layer up to 80% of the FSH, whose signal was clearly discernible before the back wall signal and thus not considered noise. Instead, the virtual electronic gate was positioned right after the pulse width of the back wall signal, measuring the nearest maximum noise indicated by the green cursor in Fig. 3(c).

Figure 4(a), (b), and (c) show the SNR values for all focal law settings, with the minimum required SNR of 3 to 1 indicated by the dashed red line. The SNR is evidently improved as the VPA size increases. Meanwhile, the gain values, at which all signals of interest are at 80% of the FSH, were recorded, and a single average gain value was calculated to maintain consistent TCG settings to be implemented for all focal law configurations. The gain values are plotted accordingly, while the calculated average gain value is denoted by the dashed green line in Fig. 4(d), (e) and (f).

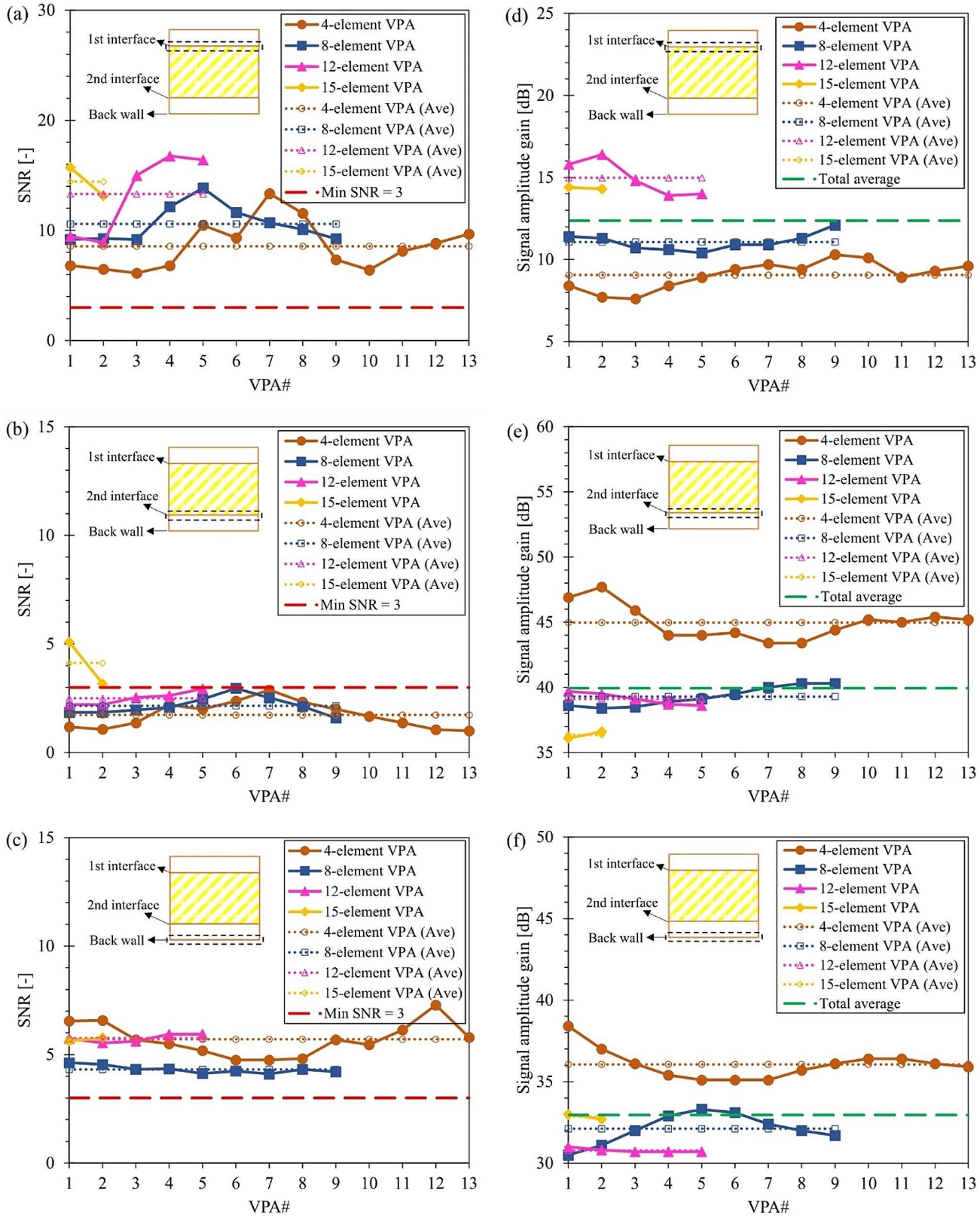

Fig. 4 SNRs (left) and signal amplitude gain in dB (right) for all focal law settings, for the signal of the ((**a**) and (**d**)) first interface layer, ((**b**) and (**e**)) second interface layer, ((**c**) and (**f**)) and back wall, respectively

Table 2 Average gain values and gain increment for TCG settings

TCG points	Position [mm]	Average gain value [dB]	Gain increment [dB]
1	0.00	12.4	+0.0
2	6.50	12.4	+0.0
3	21.50	39.9	+27.5
4	26.00	33.0	+20.6

The better detection capability and lesser signal attenuation are observed on larger VPA sizes because a lesser gain value is required to obtain detectable signals of the second interface layer and back wall.

3.1.5 TCG Settings

Initially, the instrument's gain setting was set so that the signal from the first interface layer reaches the highest level based on the calculated total average gain value of 12.4 dB, as indicated by the dashed green line in Fig. 4(d). Using the TCG function in the instrument, the gain values of the signals from the second interface layer and back wall were increased at their specific positions, known as TCG points, based on the difference between the calculated total average gain values, as indicated by the dashed green lines in Fig. 4(e) and (f), and the instrument's gain setting. The information about the gain values essential for the TCG settings is listed in Table 2.

The placement of the second TCG point was neither at the actual depth of the first interface layer, which is 5 mm, nor at the measured depth of this layer, registering slightly below the actual thickness, as shown in Fig. 5. However, it was placed approximately at the end of the pulse width in order to avoid unnecessary increment of the noise signal right afterward. The discrepancy in the thickness measurement of the outer cover layer resulted from employing an average sound velocity somewhat lower than the true sound velocity of the HDPE material, which is approximately 2,460 m/s, as specified in the instrument's guideline [26]. As a result, the time of flight for the sound wave was shorter than anticipated. In contrast, the location of the third and fourth TCG points, representing the distance of the second interface layer and back wall, respectively, were placed at the actual depth position, showing a close agreement with the measured distance. This accuracy emphasized the reliability of employing an average sound velocity for depth measurement in ultrasonic testing of TCP samples with different material compositions across multiple layers.

After implementing the necessary gain increment at the four TCG points and placing the PAUT transducer at the

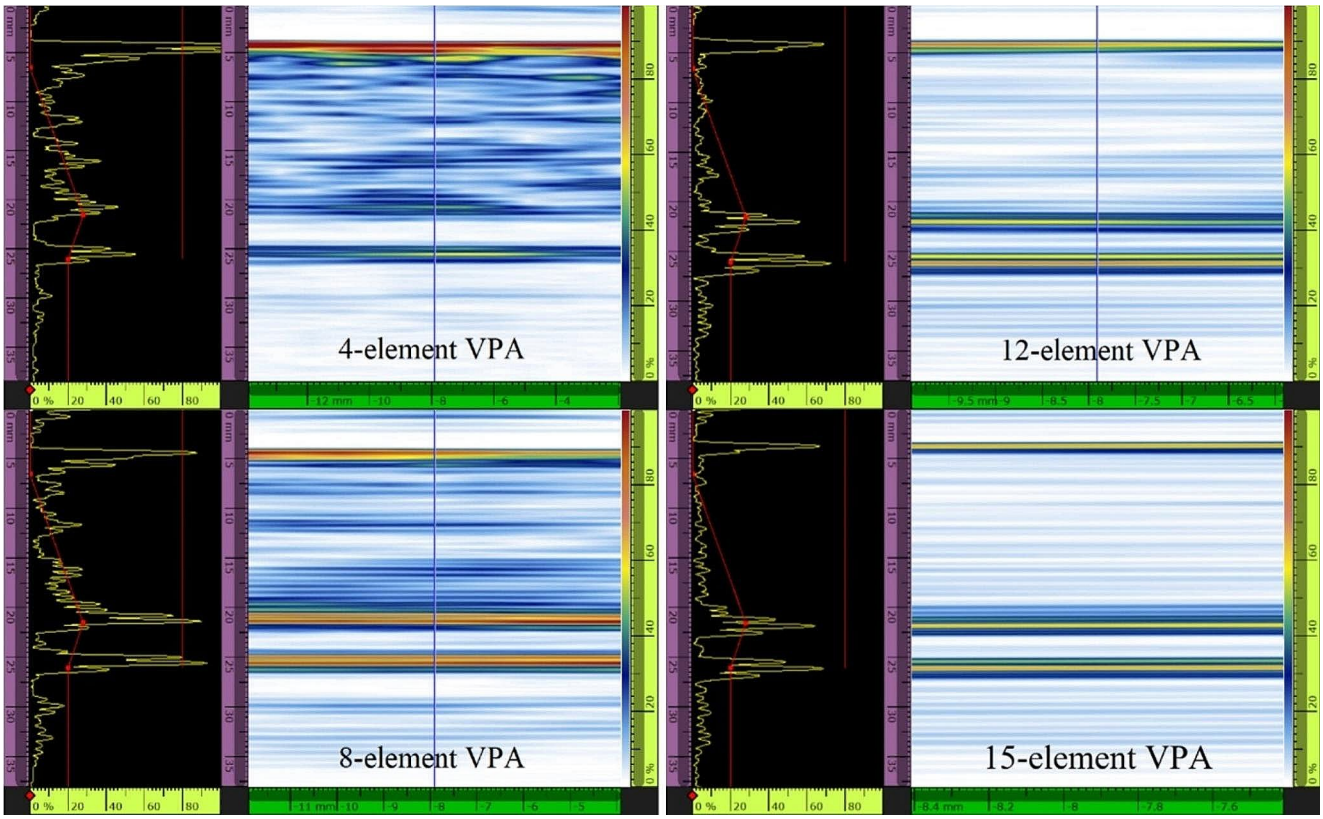

Fig. 5 A-scan (left) and E-scan (right) views for the signal of the first interface layer, the second interface layer, and the back wall at the defect-free area after implementing the TCG settings

defect-free area of the TCP sample, all signals of interest appear approximately at the same height. The TCG points are identifiable as the red points connected by the red sloping line, which are overlaid on the A-scan view located on the left side of the screen. Note that the noise signals within the laminate layer linearly increase following the implementation of the TCG settings. However, this effect reduces as the VPA size increases, which significantly improves the SNR of the signal from the second interface layer and the back wall. It is also worth noting that the pulse width of the second interface layer and the back wall also increases due to the significant gain increment, which was measured from the A-scan data to be approximately 5 mm. Hence, it would be challenging to detect defect that has an ultrasonic distance nearby to these two signals.

3.1.6 SNR Assessment After Implementing the TCG Settings

The SNRs for all three signals of interest were measured and evaluated. When comparing the SNR before and after TCG implementation for the signal of the first interface layer, the increased signal amplitude of the background noise right after the signal of the first interface layer following the TCG slope line has reduced the SNR significantly, as shown in Fig. 6(a). However, it does not jeopardize the ability to determine the true signal of the first interface layer as the SNR is still relatively much higher than 3 to 1, especially at the larger VPA size.

Meanwhile, SNRs of the signal from the second interface layer and back wall improve after implementing the TCG method and with increasing VPA size, as shown in Fig. 6(b) and (c), respectively, except for the 4-element VPA. The difference between the average signal amplitudes of all three signals of interest recorded by the 4-element VPA and the average signal amplitude for all tests used to determine the TCG points was higher than that for the rest of the larger VPAs. This difference can be visualized in Fig. 4(d), (e) and (f), where the vertical distance between the dotted line representing the average signal amplitude for the 4-element VPA, and the dashed green line, which represents the average signal amplitude of all tests used for the TCG points determination, is the farthest.

3.2 X-Ray CT Scan Method

In addition to the UT, the fabricated defect within the composite laminate layers introduced during the pipe manufacturing process was visualized in a three-dimensional view using the X-ray CT scan for qualitative and quantitative analysis. The TCP sample was scanned using a Nikon XT H 225 ST scanner with a choice of X-ray source from 180 kV transmission target to 225 kV ultra-focus reflection target, a field of view of 200 mm, and a scan resolution of 200–300 µm. The CT data were acquired and reconstructed using the Nikon in-house developed Inspect-X software. The three-dimensional volumetric data were visualized and analyzed using the open-source Imaris Viewer Software.

4 Results and Discussions

4.1 FBHs

The PAUT transducer was placed so that the FBH was positioned in the middle of the transducer's length or active aperture. The smallest 4-element VPA detected the FBH primarily by its three most centered VPAs. Hence, the data from only the three most centered VPAs for all focal law settings, except only two for the 15-element VPA, was used for the assessment.

In general, the proposed technique detected and accurately measured the depth of all FBHs, except that the smallest VPA did not detect FBH-4. Figure 7 shows the typical PAUT results on the detection of all FBHs of different depths in multi-layered TCP samples after implementing the TCG method. In addition to the ultrasonic signals from FBH-1, FBH-2, and FBH-3, the presence of ultrasonic signals from the first and second interface layers before and after them indicates that these fabricated defects are located within the composite laminate layers. The signal from the reflected backward energy within the transducer, located at approximately 16 mm in the distance, becomes apparent when FBH-1 is detected and merges with the ultrasonic signals from FBH-2 and FBH-3. Meanwhile, the signal from the FBH-4 overlaps with the signal from the second interface layer, appearing as a single, messy signal because of its location that falls within the pulse width of the second interface layer inferring that the signal resolution could not discriminate the difference of time of flight between them [7].

Relative error, e_{rel}, was used to assess the precision of distance measurement considering the average velocity used for ultrasonic wave travelling in different medium with slightly different velocity and calculated by:

$$e_{rel} = \frac{|d_{meas} - d_{act}|}{d_{act}} \times 100 \tag{2}$$

where d_{meas} and d_{act} are the measured and actual distances of the FBH, respectively. The measured depths of the FBHs, marked by the red cursors in Fig. 7, were compared with their actual depths, and the corresponding relative errors are listed in Table 3. In general, the relative error is relatively low, which is less than 6%, except for FBH-1, which reports

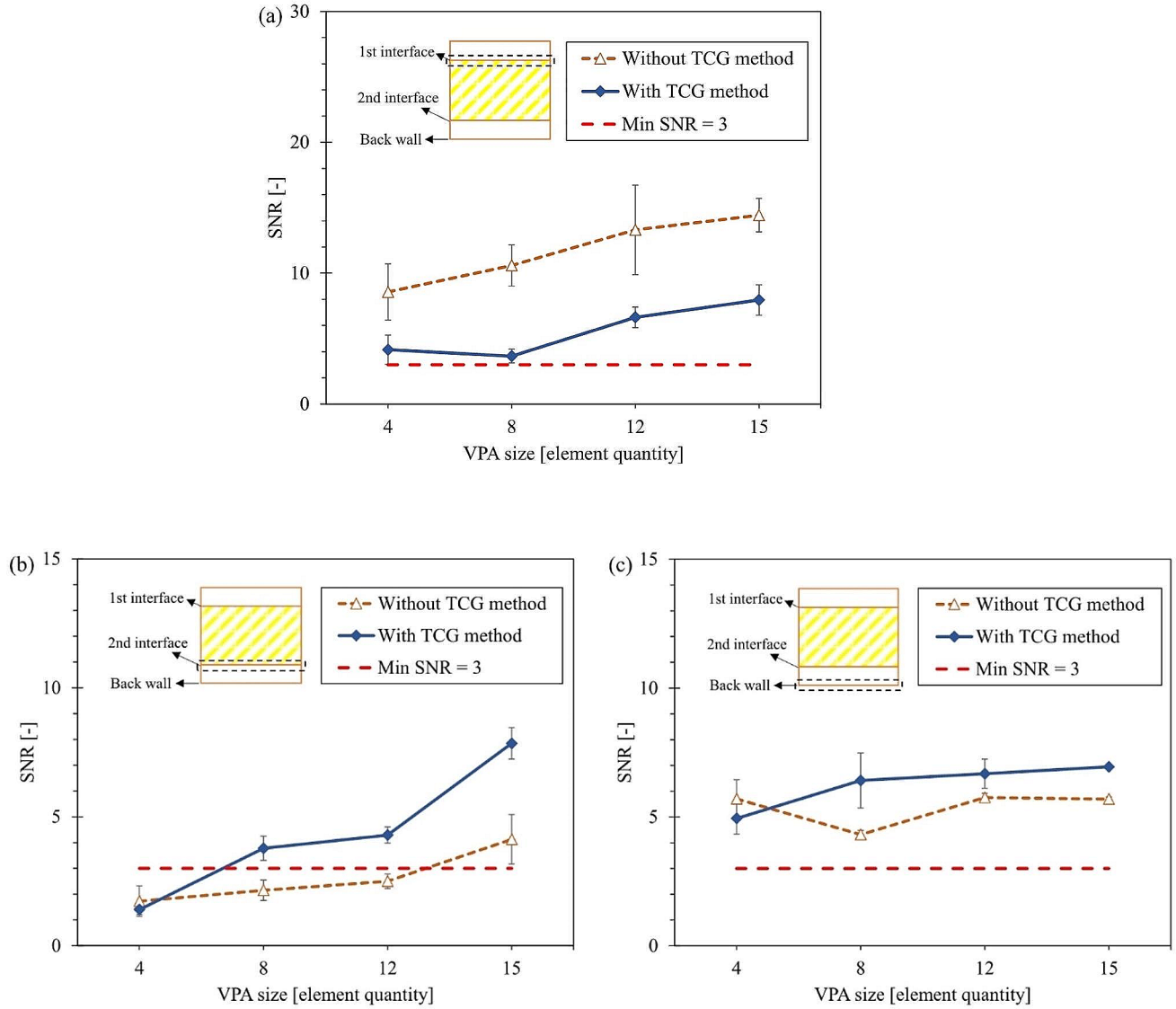

Fig. 6 Relationship between the average SNR and the VPA size before and after implementing TCG method for the signal of the (**a**) first interface layer, (**b**) second interface layer, and (**c**) back wall

a relatively high relative error of up to 9%. Nevertheless, the values are still reliable in determining the position of the defects. It is essential to highlight that without implementing the TCG method, signals originating from these FBHs might become indistinguishable from the background noise. This scenario could lead to the inadvertent selection of the wrong signal.

To further assess the effect of the VPA size in detecting the FBHs, SNRs were measured considering the defect signals and the background noise. Figure 8 shows the increasing trend of SNR with increasing VPA size. It is observed that the largest VPA records the highest SNRs for all FBHs. In general, SNRs are improved with increasing VPA size due to less unwanted beam spreading in the far-field and an achievable sharper beam focus in the near-field zones [7, 24, 27]. It is worth noting that some uncertainty factors have influenced the SNRs and depth measurement, such as average velocity in multi-layered material with slightly different sound velocities and the presence of the reflected backward energy within the transducer when the gain was significantly increased [22, 25]. SNRs for FBH-2 are higher than those of FBH-1 and FBH-3 because the location of this FBH was relatively farther away from the first and second interface layers. While the proximity of the increased reflected backward signal within the transducer caused the uncertain trend of the SNRs with increasing VPA size, the studies found that the largest 15-element VPA detected the defect with the highest SNR. This uncertainty factor could be eliminated by implementing an immersion technique so that the signal of

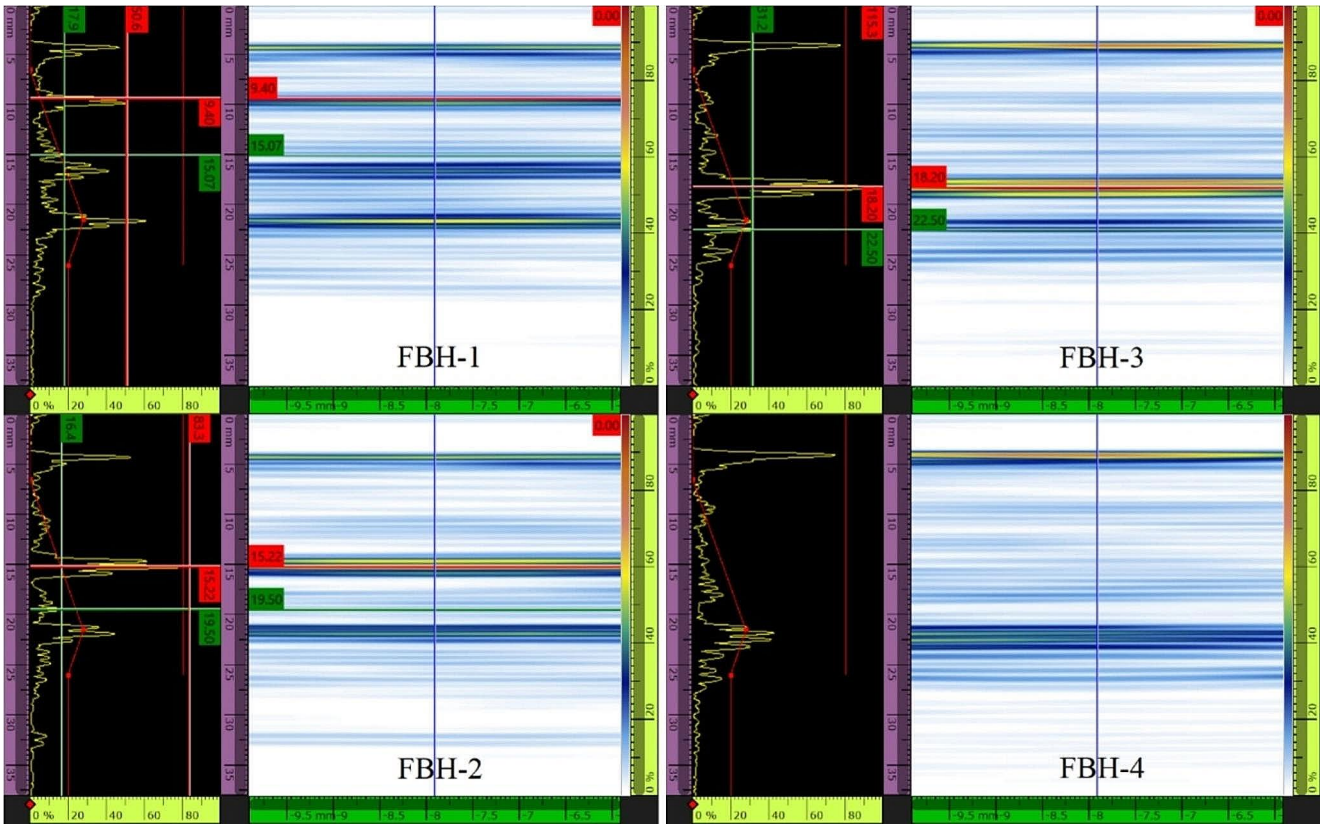

Fig. 7 Typical PAUT results on the detection of the FBHs after implementing the TCG method (Element quantity = 12)

Table 3 Distance measurements of the FBHs and their corresponding relative error to the actual value

Defect	Actual Distance [mm]	Measured Distance [mm]				Relative Error [%]			
		Element Quantity 4	Element Quantity 8	Element Quantity 12	Element Quantity 15	Element Quantity 4	Element Quantity 8	Element Quantity 12	Element Quantity 15
FBH-1	10.0	9.7	10.0	9.4	9.1	2.60	0.1	6.0	9.1
FBH-2	15.2	15.0	15.2	15.2	15.0	1.1	0.1	0.1	1.3
FBH-3	18.3	18.3	18.3	18.2	18.2	0.1	0.1	0.5	0.7
FBH-4	23.0	N/D*	22.2	22.5	22.3	N/D*	3.3	2.3	2.9

*N/D = Not Detected

interest has some added distance beyond the position of the unwanted signal occurring early in time-based view.

4.2 Fabricated Defect Within the Composite Laminate Layers

Figure 9 shows cross-sectioned radiographic images at the location of the fabricated defect within the composite laminate layers introduced during the pipe manufacturing process extracted from the three-dimensional data reconstruction obtained by the X-ray CT scan method. The radiographic images of the glass fibers are clearly distinguished from the outer cover, the matrix material within the laminate, and the inner liner layers because these two different materials have a high contrast difference due to the significant difference in density values, which plays an important role in the absorption rate of the penetrating radiation source. The relatively denser glass fibers (density $\approx$ 2.54–2.60 g/cm^3) absorbs a relatively larger amount of radiation source resulting in lesser radiation exposure on the film. As a result, the film appears to be white. On the contrary, a relatively larger amount of radiation source penetrates through the relatively less dense HDPE material (density $\approx$ 0.93–0.97 g/cm^3), resulting in darker grey radiographic images on the film.

To better visualize and characterize the defect morphology, the reconstructed volumetric data is virtually cross sectioned approximately at the center of the defect location in two perpendicular planes, as shown by Fig. 9(a) and (b). It is

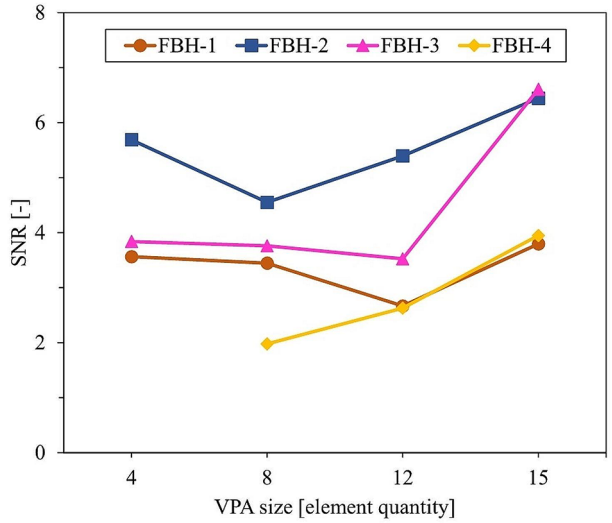

Fig. 8 Relationship between the VPA size and the average SNRs of the UT signal from all FBHs

challenging to make an accurate measurement on the three-dimensional reconstruction data obtained by the X-ray CT scan technique. Hence, the defect dimension is estimated by comparing it with the known diameter of the FBH and the physically measurable thickness of the TCP sample from the same radiographic images. From the standpoint of the PAUT transducer, the defect within the composite laminate layers resembles two upside-down truncated cones, the bigger of which is virtually stacked on top of the smaller one, with the smallest circular base, representing the deepest interface between the outer cover and the composite laminate layers, located at approximately 13.44 mm from the surface of outer cover layer, as illustrated in Fig. 10(a).

The ultrasonic B-scan representation was manually created by stacking multiple E-scan data captured at a specific distance interval along the axial length of the TCP sample in proximity of the defect. Considering the ultrasonic beam size generated by different focal law settings, the higher the number of elements pulsed together to generate a single wavefront result in a bigger VPA size, but the size of the representative received signals is averaged out to represent a smaller section of area relative to the total aperture of the active element. Hence, more overlapped E-scan data is required to generate a B-scan view for the larger VPA size in this manner. Consequently, it was challenging to manually generate a B-scan representation for the 15-element VPA using a PAUT transducer with a total of 16 active element and a 1 mm pitch used in this study because the distance interval for the index movement of the transducer must be less than 1 mm to ensure sufficient data overlapping. Additionally, a conservative approach was taken for this study by considering an overlapping of approximately half the size of the VPA in facilitating the manual generation of the B-scan representation of the defect. Hence, this approach required overlap distances of roughly 6 mm, 4 mm, and 2 mm while capturing multiple successive E-scan data of the defect, as illustrated in Fig. 10(b), (c) and (d), using the 4-, 8- and 12-element VPA, respectively.

From the B-scan view, the deepest interface between the outer cover and the composite laminate layers at the defective area, represented by the smallest circular base of the truncated cones, reflects off most of the ultrasound energy. All focal law settings recorded this location to be approximately 14.00 mm, which brings about less than 10% relative error compared to the actual position. This evidence proves again that the implementation of the average velocity in

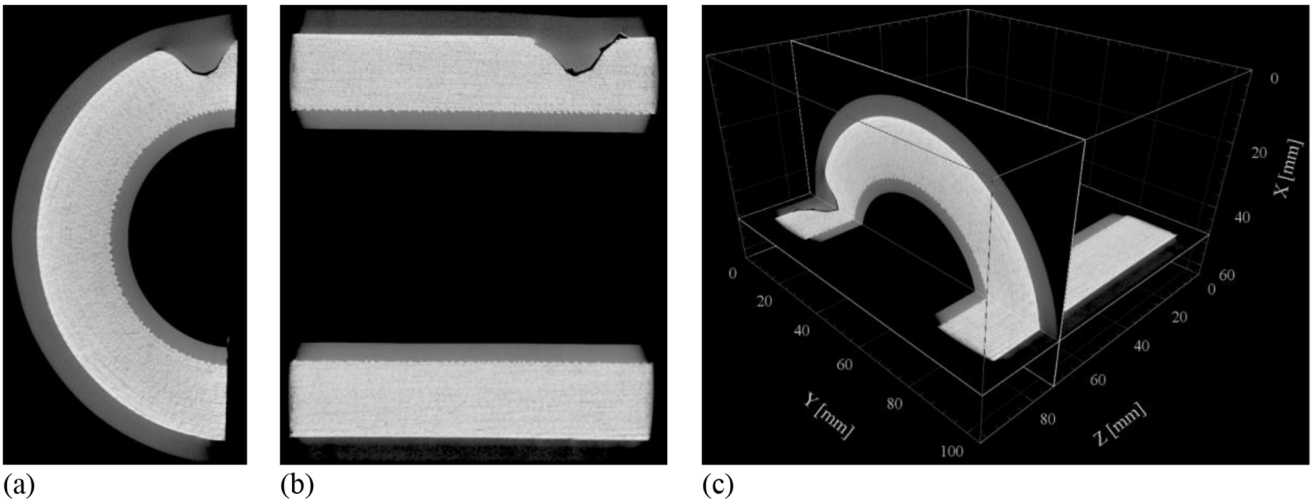

Fig. 9 X-ray CT scan volumetric reconstruction of the TCP sample indicating the morphology and location of the fabricated defect within the composite laminate layers with two cross-sectioned radiographic images on perpendicular planes from (**a**) the side and (**b**) the top view, making up (**c**) the three-dimensional view

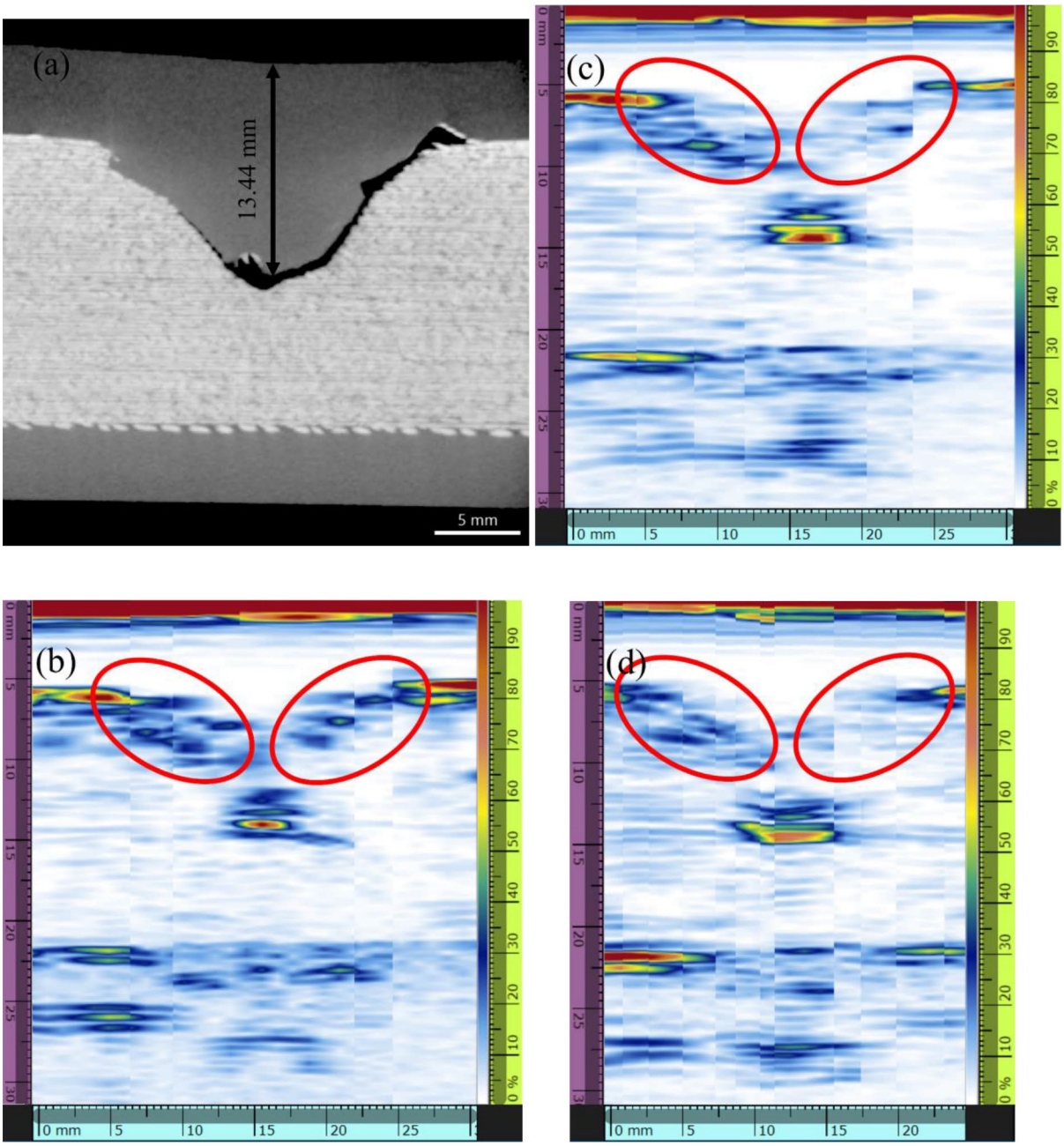

Fig. 10 Qualitative and quantitative comparison between NDT images of the fabricated defect within the composite laminate layers using (**a**) the X-ray CT scan technique (magnified view) and the manually generated B-scan representation from the PAUT results using different VPA sizes with element quantity of (**b**) 4, (**c**) 8, and (**d**) 12, respectively

the UT settings can measure the defect depth location quite accurately. Meanwhile, the size of the smallest circular base of the truncated cones is approximated by using cursor measurement in the generated B-scan view. The defect width is determined by the distance between two signals from the consecutive VPAs with amplitude at the 50% FSH or at the − 6 dB level using the vertical cursors on the screen. This distance depends on several factors, such as the pitch aperture size and the beam spread [7]. Hence, this method of measuring the defect size is less accurate than the traditional − 6 dB drop method but is still reliable for approximation only.

The smallest VPA approximates the size of the smallest circular base to be closest to the actual size based on the measurement from the radiographic image, considering only the area oriented almost horizontally to the wave propagation, which reflects off the most energy. As the VPA size increases, the defect dimension is slightly oversized

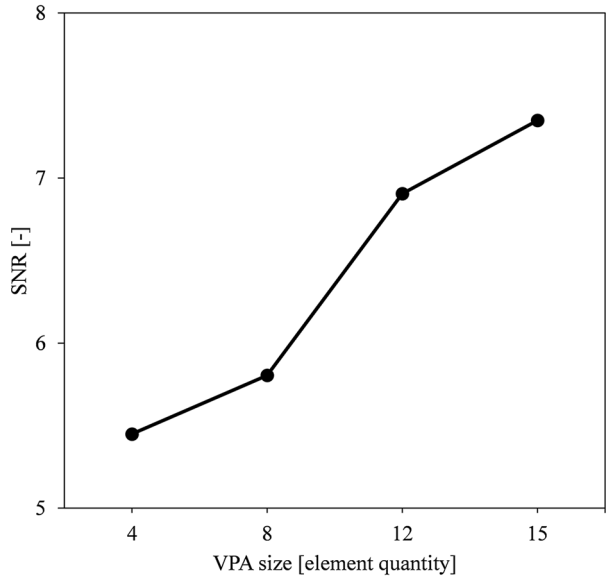

Fig. 11 Relationship between the VPA size and the SNR of the deepest interface between the outer cover and composite laminate layers at the defective area within the composite laminate layers

according to the cursor measurement, but on the other hand, the SNR improves, as shown in Fig. 11. Additionally, a relatively smaller amount of the ultrasonic energy is successfully detected after it is reflected off the less steep slant area of the top truncated cones, as circled red in Fig. 10, even though this area is unfavorably oriented to the propagating sound beam. These signals are more apparent as the VPA size is smaller. These effects imply a better sensitivity of detecting and characterizing smaller and irregular defects when using a smaller VPA but a better SNRs when using a larger VPA.

A destructive testing approach was eventually taken during this study by cross-sectionally cutting the TCP sample at the defective area for visual testing and comparison with the results recorded by both NDT techniques. Figure 12 shows the cross-sectional view of the TCP sample approximately at the center part of the defect within the composite laminate layers. It is noted that the gap within the removed part of the composite laminate layers is filled with the HDPE material of the outer cover layer. Even though this study shows a good agreement between the results from both NDT techniques in detecting the irregular defect, it is inarguably proven that the imaging-based technique using the more advanced X-ray CT scan provides the most accurate representation of the actual defect, compared to the ultrasonic wave-based technique. However, the practical application of the X-ray CT scan in the field is still challenging to inspect a kilometer-long pipe since the inspection setup would require either the whole test setup or the test object itself to be rotated while capturing multiple two-dimensional radiographic images for the three-dimensional reconstruction images.

Based on the results of the two NDT techniques used in this study, the presence of fabricated defects within the TCP samples comprised of multiple layers of dissimilar compositions can reliably be detected and characterized quite accurately. With the implementation of the classical TCG method, the UT technique could almost precisely locate and size the defect beyond the first interface layer, which was

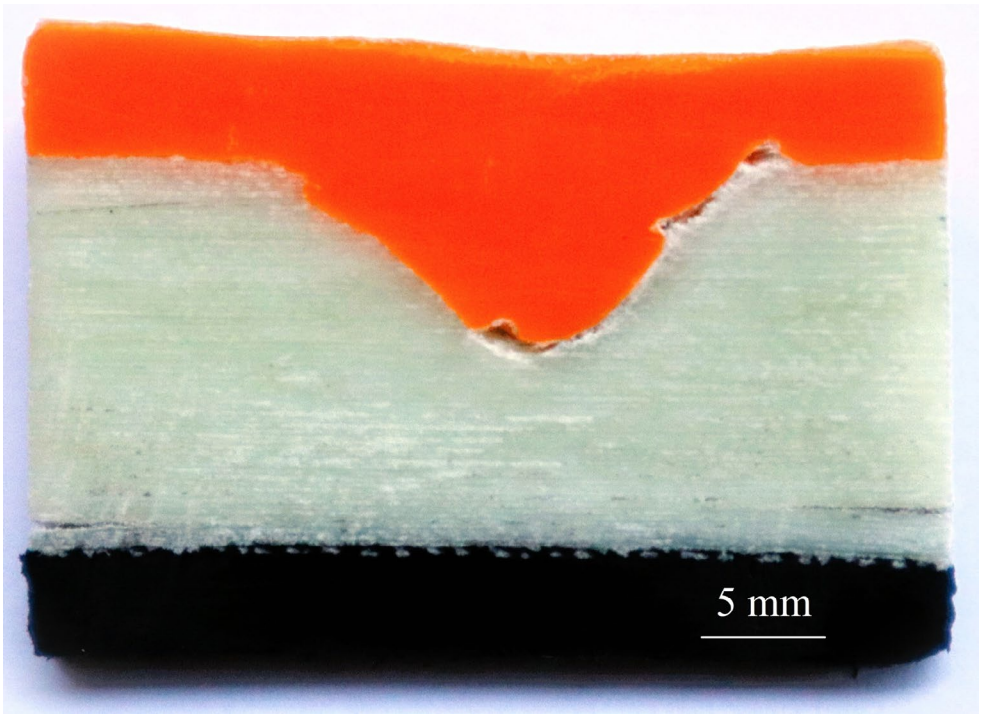

Fig. 12 Cross-sectional view of the TCP sample at the defective area within the composite laminate layers introduced during the pipe manufacturing

confirmed by the more accurate imaging-based radiographic technique. While the FBH resembles one-sided delamination within the composite laminate layers, the fabricated defect within the composite laminate layers, which is invisible from the outside, has some similarity with the barely visible impact damage should an external force strike the pipe. It is believed that the proposed method should be ready to be applied in the field for detection and characterization of typical actual defects in TCP, like delamination within the composite laminate layers and thinning of the outer cover or inner liner layers due to yielding or erosion. This study will be incorporated into the future works.

5 Conclusions

This paper presented the feasibility of detecting defects in thick multi-layered TCP samples utilizing the PAUT technique implementing the classical TCG method to compensate for the severe spatial signal attenuation beyond the first interface layer. The sound wave velocity was calibrated directly on the TCP sample, using the two-point calibration method, and referring to the known depths of the two interface layers and the back wall. Since the sound wave was traveling at slightly different velocities within materials of different compositions, the calibrated value of sound velocity in this manner is considered an average value.

In addition to the implementation of the classical TCG method, the effect of different VPA size by grouping and pulsing a different number of elements together to generate and receive a single wavefront in detecting the FBHs was studied. Despite using an averaged velocity, the location of the FBHs was recorded quite accurately, with mostly calculated to be less than 6% relative error. Meanwhile, the increment in the VPA size showed an increasing trend of the SNR. The proposed method was then applied to detect the irregular defect within the composite laminate layers introduced during the pipe manufacturing process. X-ray CT scan technique was also used to better visualize the morphology of this defect. The result from the radiographic technique was qualitatively and quantitatively compared with the results of the PAUT technique, and they both showed a good agreement.

Even though the advanced X-ray CT scan technique can provide the most accurate representation of the actual defect compared to the PAUT technique, the practical application in the field is very challenging because either the whole test setup or the kilometer-long pipe must be rotated to capture multiple two-dimensional radiographic images, from which virtual slice images will be reconstructed to generate a three-dimensional data. In contrast, the PAUT technique with the implementation of the classical TCG method is readily available for application in the field.

Acknowledgements This work is part of the DNV-led Joint Industry Project called Composite Pipe Integrity Management System (C-PIMS) with 12 industrial partners and the Norwegian University of Science and Technology (NTNU).

Author Contributions Mohd Fadzil Mohd Tahir: Conceptualization, Investigation, Methodology, Validation, Visualization, Writing ? original draft preparation, Writing ? review and editing. Andreas T. Echtermeyer: Conceptualization, Funding acquisition, Methodology, Resources, Writing ? review and editing.

Funding This work was funded by the Research Council of Norway (Project No. 309238) in the PETROMAKS programme.
Open access funding provided by NTNU Norwegian University of Science and Technology (incl St. Olavs Hospital - Trondheim University Hospital)

Data Availability The datasets generated and analyzed during the current study are available from the corresponding author on reasonable request.

Declarations

Ethical Approval Not applicable.

Consent to Participate Not applicable.

Consent for Publication All authors consent to publish this work.

Competing Interests The authors have no relevant financial or non-financial interests to disclose.

References

1. Onna, M.V.: TCP Sustainability #3: TCP the best solution for offshore hydrogen infrastructure. (2021). https://strohm.eu/articles/tcp-sustainability-3-tcp-the-best-solution-for-offshore-hydrogen-infrastructure. Accessed 3 February 2023
2. Skopljak, N.: Thermoplastic composite pipes significantly more eco-friendly than carbon steel pipes, report says. (2022). https://www.offshore-energy.biz/thermoplastic-composite-pipes-significantly-more-eco-friendly-than-carbon-steel-pipes-report-says/. Accessed 2 February 2023